Energy Advances

ROYAL SOCIETY OF CHEMISTRY

PAPER

View Article Online
View Journal | View Issue

Cite this: *Energy Adv.*, 2025, 4, 400

The impact of double crosslinking and alkaline activation strategies on the multifaceted characteristics of quaternized poly(vinyl alcohol) anion exchange membranes

Wei Keat Ng,[a] Chun Yik Wong,[b] Nur Adiera Hanna Rosli,[a] Kiranraj Vaiyanan Kannan,[a] Kee Shyuan Loh,[a] Bee Lin Chua[c] and Wai Yin Wong *[a]

This study investigates the effects of crosslinking strategies and KOH activation on the multifaceted characteristics of quaternized poly(vinyl alcohol) (QPVA) membranes for anion exchange membrane (AEM) applications. *In situ* and combined *in situ*/*ex situ* crosslinking with glutaraldehyde were evaluated at 5 M, 6 M, and 8 M KOH concentrations. Multifaceted characteristics on the membranes including ionic conductivity, swelling degree, thermal and oxidative stability are studied. Four types of membranes: M1 (*in situ* crosslinked, heated), M2 (*in situ* crosslinked, no heating), M1 2x (*in situ*, heated and *ex situ* crosslinked), and M2 2x (*in situ*, no heating and *ex situ* crosslinked) were synthesized. The M1 5 M KOH membrane (*in situ* crosslinked, heated activation) demonstrated the highest ionic conductivity (40.93 mS cm^{-1} before equilibrium, 33.41 mS cm^{-1} after equilibrium) and moderate oxidative stability (81.10%). Combined crosslinking and higher activation temperatures improved the membrane stability and mechanical properties but reduced the oxidative stability owing to potential alkaline attack on glutaraldehyde crosslinked groups. Oxidative stability is critical for AEMs because they are exposed to reactive oxygen species (ROS) generated during fuel cell operation or electrolysis. Poor oxidative stability can lead to degradation of the membrane, reducing its lifespan and overall performance in these applications. The novelty of this work lies in the dual crosslinking strategy, which significantly enhances the mechanical and thermal properties of QPVA membranes, while also highlighting the impact of KOH activation on crystallinity and ion transport. This study emphasizes the importance of optimizing crosslinking and activation conditions to develop high-performance QPVA membranes for energy conversion and storage applications such as fuel cells and electrolyzers.

Received 30th September 2024,
Accepted 27th December 2024

DOI: 10.1039/d4ya00555d

rsc.li/energy-advances

1. Introduction

Green hydrogen is viewed as the next-generation fuel source to replace non-renewable fossil fuels. It offers great promise for meeting the world's energy demands, with nearly 94 million tons of hydrogen produced in 2021, equivalent to about 2.5% of global total energy consumption.[1] Among various types of fuel cells, alkaline exchange membrane fuel cells (AEMFCs) have developed rapidly in recent years due to their advantages of sharing most of the structural features of proton exchange membrane fuel cells (PEMFCs). Additionally, operating at a higher pH, AEMFCs have a less corrosive environment and exhibit higher tolerance to affordable materials in cell components, including bipolar plates, membranes, and catalysts.[2]

To facilitate reactions in AEMFCs, anion exchange membranes (AEMs) are crucial for conducting anions (OH^-) while preventing corrosion and leakage issues associated with liquid electrolytes.[3] To date, a wide range of cationic fixed charge groups have been extensively studied, including quaternary ammonium,[4,5] quaternary phosphonium,[6,7] quinuclidinium-based quaternary ammonium,[8,9] imidazolium,[10,11] pyridinium,[12] and pentamethyl guanidinium groups.[13] Among these, AEMs with ammonium groups exhibit higher thermal and chemical stability compared to phosphonium or sulfonium groups.[14] However, the literature indicates that phosphonium groups in AEMs are more susceptible to free radical attacks by OH^- ions than quaternary ammonium groups.[15]

In this work, poly(vinyl alcohol) (PVA) was selected as the primary polymer due to its low cost, excellent mechanical

[a] *Fuel Cell Institute, Universiti Kebangsaan Malaysia, 43600 Bangi UKM, Selangor, Malaysia. E-mail: waiyin.wong@ukm.edu.my*
[b] *Clean Energy Research Center, University of Yamanashi, Kofu, 400-8510, Japan*
[c] *Department of Engineering, School of Engineering and Technology, Sunway University, Jalan Universiti, Bandar Sunway, 47500 Petaling Jaya, Selangor, Malaysia*

properties, solvent resistance, flexibility, good film-forming ability, hydrophilicity, and abundant reactive functional groups for facile crosslinking through irradiation and thermochemical reactions.[16,17] Notably, PVA's high dielectric constant and glass transition temperature are key advantages for fuel cell applications. Following early research on PVA for AEMs, Lewandowski *et al.*[18] proposed using potassium hydroxide (KOH) and water (H_2O) as dopants to introduce functional ion sources for ion diffusion. The addition of KOH to PVA resulted in the formation of alcoholates, which contributed to the conductivity of the solid electrolyte. Nevertheless, high conductivity alone is insufficient for practical AEM applications. Parameters such as electrochemical and dimensional stability are also essential considerations. Subsequently, various researchers attempted to quaternize PVA. The low quaternization degree of QPVA often leading to low ionic conductivity has been addressed through polymer blending or incorporating ion-conductive fillers. Notably, reported hydroxide ion conductivities for QPVA-based membranes range from 5 mS cm^{-1} to a maximum of approximately 50 mS cm^{-1}.[3,19] Despite advancements in ionic conductivity as reported by Samsudin *et al.*,[19] dimensional swelling remains a significant challenge.

Zakaria *et al.*[20] reported an ionic conductivity of 4.7 mS cm^{-1} for a QPVA membrane. Polymer crosslinking is a common technique for enhancing the mechanical performance of polymer-based composites.[21] It involves forming covalent bonds between polymer chains, strengthening the polymer matrix.[22] Crosslink density, determined by the number of crosslinks, influences the polymer network. Increasing the crosslink density reduces the free volume, leading to improved thermal stability but potentially hindering ion diffusion and reducing conductivity.[23] Liao *et al.* demonstrated this trade-off by achieving low ionic conductivity after crosslinking QPVA/Q-chitosan with GA at 85 °C using HCl as a catalyst for 3 hours. Optimizing crosslinking conditions is crucial for balancing conductivity, electrochemical stability, and dimensional stability. Recent advancements in PVA-based and other anion exchange membranes highlight the importance of tailored crosslinking strategies. For example, dual crosslinked PVA membranes demonstrated excellent ion selectivity and mechanical stability, as reported by Mu *et al.*[24] Similarly, ionic liquid-grafted membranes incorporating long side-chain N-heterocyclic cations were shown to exhibit superior ionic conductivity and alkaline stability, making them highly suitable for fuel cell applications.[25] Furthermore, covalently crosslinked membranes have been successfully applied in low-temperature ammonia fuel cells, offering enhanced performance under operational conditions.[26]

In situ crosslinking is a technique where crosslinking occurs during the polymer processing or membrane casting stage, allowing the reaction to take place directly within the polymer matrix. *In situ* crosslinking of PVA with glutaraldehyde (GA) is well-studied, often involving acid catalysis.[19,27] In the case of PVA, *in situ* crosslinking with glutaraldehyde (GA) involves the reaction of aldehyde groups in GA with hydroxyl groups in PVA to form stable acetal linkages. This method is typically catalyzed by acids to accelerate the reaction and achieve uniform crosslinking throughout the membrane. However, acid catalysis can lead to degradation in alkaline environments, making it unsuitable for applications like AEMs operating under high pH conditions.[28] To overcome this, our study employs an acid-free *in situ* crosslinking approach, enabling better control over reaction kinetics and ensuring membrane stability in alkaline conditions. External crosslinking, where the membrane is immersed in a crosslinking solution, offers advantages like thinner membranes with improved properties.[29] However, it has not been applied to QPVA membranes to our knowledge. To address these challenges, we combined *in situ* and *ex situ* crosslinking while avoiding acid catalysis. Additionally, we explored the effects of high KOH concentration activation on conductivity and other properties.[30]

The novelty of this study lies in the dual crosslinking strategy, combining *in situ* and *ex situ* crosslinking methods, which significantly enhances the mechanical properties and thermal stability of QPVA membranes while maintaining high ionic conductivity. Furthermore, the effect of high KOH concentration activation on membrane crystallinity and ion transport is investigated, a factor that has not been previously explored in QPVA-based anion exchange membranes. This study aims to investigate the impact of crosslinking strategies on QPVA-based AEMs. We synthesized four types of membranes: M1 (*in situ* crosslinked, heated), M2 (*in situ* crosslinked, no heating), M1 2x (*in situ*, heated and *ex situ* crosslinked), and M2 2x (*in situ*, no heating and *ex situ* crosslinked). We evaluated their ionic conductivity, IEC, oxidative stability, and mechanical properties. The influence of different KOH concentrations on membrane performance were also examined.

2. Experimental

2.1. Materials

Poly(vinyl alcohol) powder (PVA, 99.5% hydrolysed, M_w = 85 000–124 000 g mol^{-1}, Sigma-Aldrich, United States), glycidyltrimethylammonium chloride (GTMAC, ≥90%, Sigma-Aldrich, United States), anhydrous ethanol (absolute for analysis EMSURE® ACS, Sigma-Aldrich, United States), glutaraldehyde (GA, 25% in H_2O, Sigma-Aldrich, United States), potassium chloride pellets (KOH, ≥85% ACS reagent, Sigma-Aldrich, United States), hydrochloric acid fuming (HCl, 37% for analysis EMSURE® ACS, Merck Millipore), and sodium hydroxide pellets (NaOH, AR Grade, Macron Fine Chemicals, United States) were used. For sample preparation and analytical testing, deionised water was used throughout the experiment.

2.2. Preparation of quaternized poly(vinyl alcohol)

Prior to QPVA preparation, PVA solution was first prepared by dissolving PVA resin in deionized (DI) water at 90 °C for approximately 2 hours under vigorous stirring. Subsequently, the solution temperature was reduced to 65 °C with continuous stirring until a transparent solution was obtained. Next, appropriate amounts of GTMAC and KOH were added, and further stirred for 4 hours until a homogeneous and colourless solution

was obtained.[27] Excess absolute ethanol was added to the resulting solution for the formation of QPVA precipitates. The yellow precipitates of QPVA were then dried in a vacuum oven to remove both moisture and any residual ethanol. Finally, the dried QPVA was dissolved in DI water at 90 °C until a transparent solution was obtained.

2.3. Preparation of quaternized poly(vinyl alcohol) membranes

Crosslinked QPVA membranes were prepared by incorporating 20 vol% glutaraldehyde (GA) into 7 wt% QPVA solution in DI water, which was stirred until a homogeneous mixture was achieved. This process initiated covalent bond formation between the polymer chains. The resulting solution was cast onto Petri dishes, dried at 60 °C for three days, and then cured in two steps: at 80 °C for 2 hours, followed by 100 °C for 1 hour. The membranes were then activated with high-concentration KOH at either 60 °C (M1) or room temperature (28 °C) (M2) for 24 hours.[27] For the combined crosslinking process, the M1 and M2 membranes were further immersed in a GA solution (1 : 10 GA) at room temperature for 2 hours, resulting in the M1 2x and M2 2x membranes, respectively. After activation, the KOH concentration was equilibrated to 1 M before conducting analyses.

In the case of the M1 membranes, the higher activation temperature of 60 °C enhanced the mobility of the polymer chains, facilitating more effective interactions between the PVA hydroxyl groups and GA. This led to a denser and more homogeneous crosslinked network. The thermal energy provided during the 60 °C activation step promoted a higher crosslink density, which contributed to improved mechanical stability and a more rigid membrane structure. In contrast, the M2 membranes, activated at room temperature, exhibited a less efficient crosslinking network. The lower temperature restricted the mobility of the polymer chains, reducing the interaction between the crosslinking agent (GA) and the PVA matrix. As a result, the M2 membranes displayed a lower crosslink density, leading to a more irregular and less stable polymer structure. These structural differences are depicted in Fig. 1, where the M1 membranes show a smoother and more uniform crosslinked pattern, while the M2 membranes exhibit irregularities and micro-defects due to insufficient crosslinking. Fig. 1 also outlines the entire preparation and crosslinking process for QPVA membranes, including the mechanisms of quaternization and crosslinking.

2.4. Characterisation of quaternised poly(vinyl alcohol) membranes

Successive quaternization was analyzed using Fourier-transform infrared (FTIR) spectroscopy (Spectrum 100 FT-IR Spectrometer, PerkinElmer, USA) in attenuated total reflectance (ATR) mode, with a wavelength range of 4000–650 cm^{-1}. The crystalline properties of QPVA membranes were evaluated through X-ray diffraction (XRD) patterns (Bruker D-8 advanced X-ray diffractometer) using nickel-filtered CuKα radiation, scanning from 5° to 80° at a rate of 0.025° s^{-1}. The microstructures of the membranes were observed by scanning electron microscopy (SEM) (Carl Zeiss LEO 1450VP, Germany) after freeze-fracturing and gold sputtering. Thermal stability of QPVA membranes was determined using thermogravimetric analysis (TGA) (TGA 8000, Pyris 1 TGA, PerkinElmer, USA) under a nitrogen (N_2) atmosphere, heating from 35 °C to 600 °C at 10 °C min^{-1}. Prior to TGA measurements, the membranes were dried in a vacuum oven at 90 °C for 24 hours to remove residual moisture, given the hygroscopic nature of PVA.[31] Dynamic mechanical analysis (DMA) (DMA Q800, PerkinElmer, USA) were performed in a temperature sweep mode, where the samples were subjected to a heating rate of 10 °C min^{-1} from 25 °C to 200 °C to monitor the changes in the storage modulus (G') and $\tan\delta$. The frequency was set at 1 Hz, and the applied strain was kept low enough to remain within the material's linear viscoelastic region.[32]

The membrane samples were dried at 70 °C for 6 h to achieve a constant weight. The weight the dry membranes were recorded. The dried samples were then immersed in DI water for 12 hours under ambient conditions. Then, the samples were taken out, the excess water on the surface was removed with tissue paper, and the weight of the wet membrane was immediately measured.[33] The water uptake was calculated using eqn (1).

$$\text{Water uptake} = \frac{W_{\text{wet}} - W_{\text{dry}}}{W_{\text{dry}}} \quad (1)$$

where W_{wet} is the weight of the membrane after being immersed into DI water; W_{dry} is the weight of the membrane in the dry state.

The swelling degree was measured to assess membrane dimensional stability, crucial for evaluating structural integrity during operation. A higher swelling degree indicates greater deformation. It was calculated as the difference in membrane length before and after immersion in KOH, according to eqn (2):

$$\text{Swelling degree} = \frac{l_{\text{wet}} - l_{\text{dry}}}{l_{\text{dry}}} \quad (2)$$

where l_{wet} is the length of membrane after being immersed into KOH; l_{dry} is the length of membrane in the dry state.

Ion exchange capacity (IEC) was determined through acid–base titration. Dried membranes were equilibrated in 1.0 M KOH solution for 24 hours, followed by immersion in 0.1 M HCl for 24 hours. The solution was titrated with 0.1 M NaOH using phenolphthalein as an indicator. IEC values were calculated using eqn (3):

$$\text{IEC}\left(\text{mequiv g}^{-1}\right) = \frac{C_{\text{HCl}} \times (V_{\text{blank}} - V_{\text{NaOH}})}{W_{\text{dry}}} \quad (3)$$

where C_{HCl} is the concentration of HCl, V_{blank} is the volume of NaOH used to titrate a blank solution of HCl (40 mL) without the presence of immersed membrane, V_{NaOH} is the volume of titrated NaOH solution and W_{dry} is the weight of dry membrane.

Hydration number (λ) was measured to quantify the amount of water adsorbed per unit volume of the membrane by

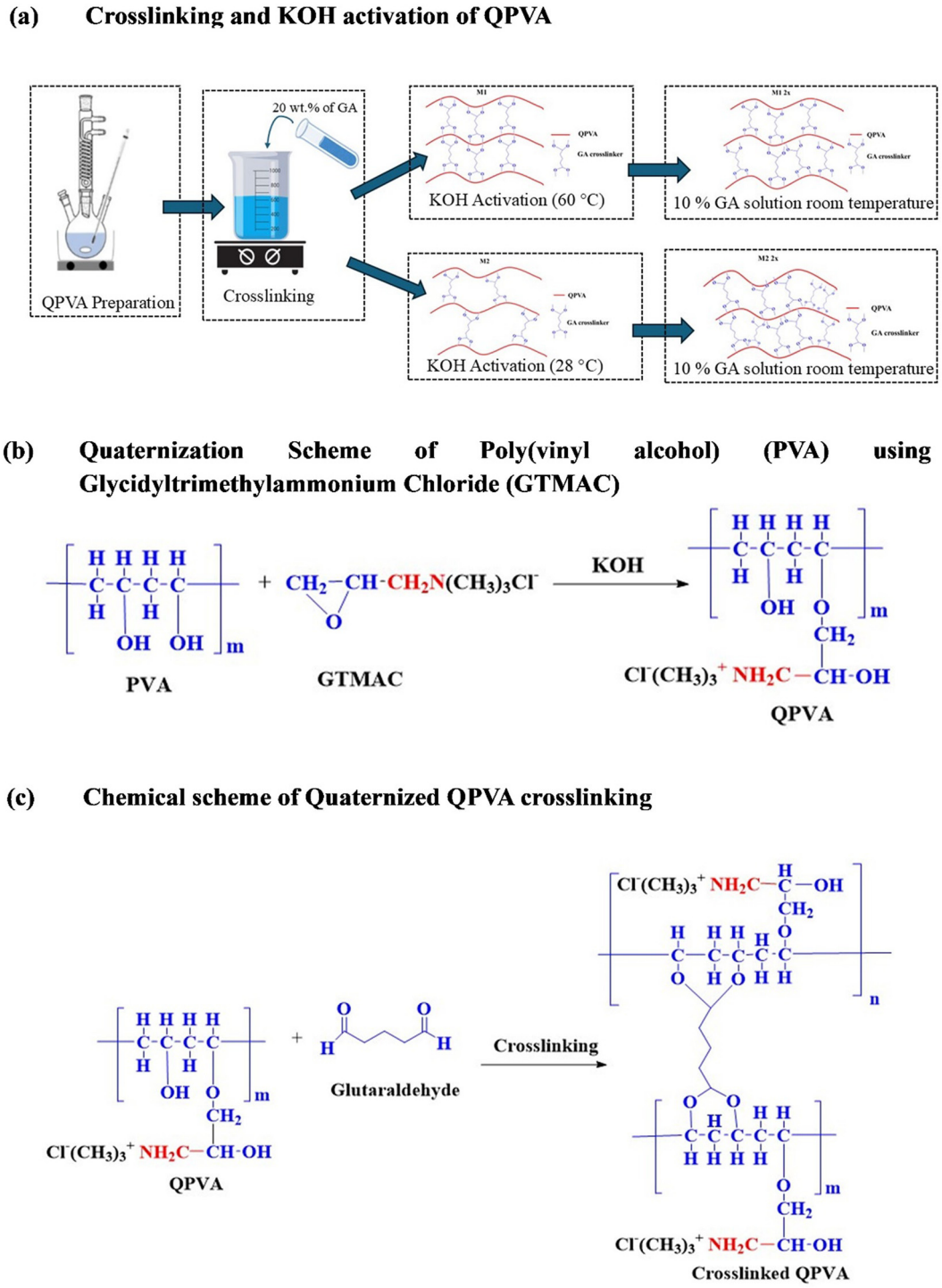

Fig. 1 Schematic representation of the synthesis and crosslinking process for QPVA membranes, including: (a) an overview of the preparation steps; (b) the quaternization scheme of poly(vinyl alcohol) (PVA) using glycidyltrimethylammonium chloride (GTMAC); and (c) the chemical scheme of quaternized QPVA crosslinking.

normalizing the water uptake (WU) capacity with the ion exchange capacity (IEC) values.[34] λ values were calculated using eqn (4):

$$\text{Hydration number } (\lambda) = \left[\frac{\text{Water uptake}}{18.01}\right]\left[\frac{10}{\text{IEC}}\right] \quad (4)$$

The molecular weight of water, 18.01 g mol^{-1}, was used in this context.

The oxidative stability of the membranes was investigated by measuring the residual weight percentage of each after Fenton's reagent treatment. The membranes with size of 2.5 × 2.5 cm^2 were dried in an oven at 60 °C for 24 hours.

The weight of the dry membrane was measured. The completely dried membranes were immersed in Fenton's reagent solution (3 wt% H_2O_2, 3 ppm Fe^{2+} of $FeSO_4$) (50 mL) for 24 hours. The membranes were then taken out from the solution and were wiped with tissue paper to remove excess moisture. Then, the membranes were dried in an oven at 60 °C for 24 hours and the weight of the dried membranes were measured. The oxidative stability (%) was calculated using eqn (5).

$$\text{Oxidative stability} = \frac{W_{\text{initial}} - W_{\text{final}}}{W_{\text{initial}}} \times 100\% \quad (5)$$

where W_{initial} is the weight of dried membranes before treatment, and W_{final} is the weight of dried membranes after treatment.

Membrane conductivity was measured using AC impedance spectroscopy with a two-probe electrochemical analyzer. Prior to testing, membranes were equilibrated in 1 M KOH solution for 24 hours at room temperature. Impedance spectra were collected over a frequency range of 0.1 Hz to 1 MHz with a 0.01 V oscillating voltage. Membrane ionic conductivity (λ) was calculated from impedance data using eqn (6).

$$\lambda = \frac{t}{A \times R_s} \quad (6)$$

where λ is the conductivity, S cm^{-1}; t is the thickness of the blended composite membrane, cm; A is the area of the blended composite membrane covered by the measurement cell, cm^2; and R_s is the electrolyte resistance, Ω.

3. Results and discussion

3.1. Characterization of QPVA membranes

FTIR spectroscopy confirmed the successful grafting of quaternary ammonium groups onto the PVA polymer chains. Fig. 2 presents FTIR spectra for the various QPVA membranes. Key absorption peaks at 3300 cm^{-1} (O–H stretching), 2906 cm^{-1} (C–H stretching), 1418 cm^{-1} (CH_2 stretching), and 1088 cm^{-1} (O–H stretching) are characteristic of the PVA structure. The appearance of new peaks at 1331 cm^{-1} and 836 cm^{-1} attributed to C–N stretching indicates successful quaternization.[35] Additionally, a peak at 2940 cm^{-1} associated with the C–O–C group in the aldehyde suggests the presence of GA.[27,36] The intensified peak at 1109 cm^{-1} (C–O–C stretching) indicates successful crosslinking with GA, involving the formation of covalent bonds between PVA hydroxyl and GA aldehyde groups, increasing crosslink density.[37]

After KOH activation, the disappearance of the 1562 cm^{-1} peak (N–H bending) and the emergence of a new peak at 1376 cm^{-1} (C–N stretching) were observed. The appearance of the 1376 cm^{-1} peak is attributed to the formation of quaternary ammonium groups, which are introduced during the quaternization process. These groups contain C–N bonds, and the C–N stretching vibrations are characteristic in the range

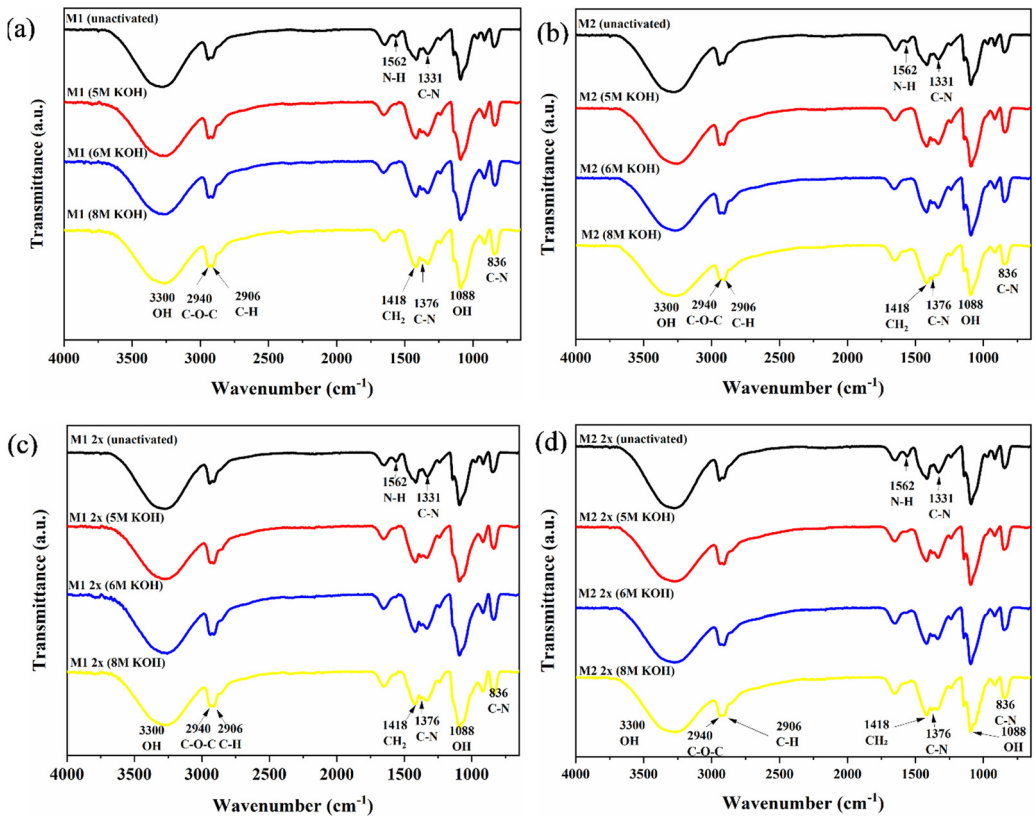

Fig. 2 FT-IR spectra of QPVA membranes (a) M1, (b) M2, (c) M1 2x and (d) M2 2x samples.

1300–1400 cm^{-1}. The emergence of this peak signifies successful quaternization, where PVA is modified to incorporate quaternary ammonium cations, enhancing the membrane's ion exchange capacity and stability. The quaternary ammonium groups formed are stable under alkaline conditions, contributing to improved ionic conductivity and thermal stability of the membrane.[38] The emergence of the 1376 cm^{-1} peak signifies the formation of a more ionically conductive membrane structure, directly contributing to improved ion exchange capacity and stability in the membrane under alkaline conditions. Similar findings by Gu *et al.*[39] support this observation. These changes contribute to improved ionic conductivity and thermal stability.

XRD analysis was performed to observe the crystalline structure of the QPVA membranes (as shown in Fig. 3). The diffraction patterns showed a peak at around 2θ of 19°, corresponding to the formation of small KOH crystals on the QPVA membrane surface. Additionally, for all samples, crystallinity increased with higher KOH concentrations. The area under this peak increased with higher KOH concentrations, indicating an increase in crystallinity. The combined crosslinking approach (M1 2x and M2 2x) led to a further increase in the peak area, reflecting higher crystallinity compared to single-step crosslinking methods. However, M2 and M2 2x samples showed greater peak area and more pronounced KOH crystal formation on the surface than M1 and M1 2x samples. A combined crosslinking approach (M1 2x and M2 2x) further increased crystallinity compared to single-step crosslinking methods. Excessive KOH crystallization on the membrane surface can detrimentally affect overall performance. These KOH crystals can block ion transport pathways, reducing ionic conductivity and negatively impacting membrane efficiency. While the formation of quaternary ammonium groups and the activation of QPVA can enhance ion transport capabilities, excessive KOH crystallization can hinder performance.[40]

SEM images illustrating the morphologies of QPVA membranes synthesized using different crosslinking techniques are shown in Fig. 4. The membranes were subjected to varying KOH solution concentrations (5 M, 6 M, and 8 M) and crosslinking methods (*in situ* with heating, *in situ* without heating, and combined crosslinking approach). M1 samples (*in situ* crosslinked with 60 °C activation) exhibited a uniform and smooth surface morphology across all KOH concentrations. This smoothness can be attributed to the homogeneous distribution of crosslinking agents within the polymer matrix, resulting in a controlled and even crosslinking process. The surface robustness of the QPVA membrane was maintained as the KOH concentration increased from 5 M to 8 M, indicating effective stabilization by the *in situ* crosslinking method even at higher alkaline concentrations.

M2 samples also displayed a relatively smooth surface morphology. However, minor irregularities and KOH crystals were present, suggesting less efficient crosslinking compared to 60 °C activation. These irregularities became slightly more pronounced with increasing KOH concentration, but the overall surface remained fairly uniform. While less effective than

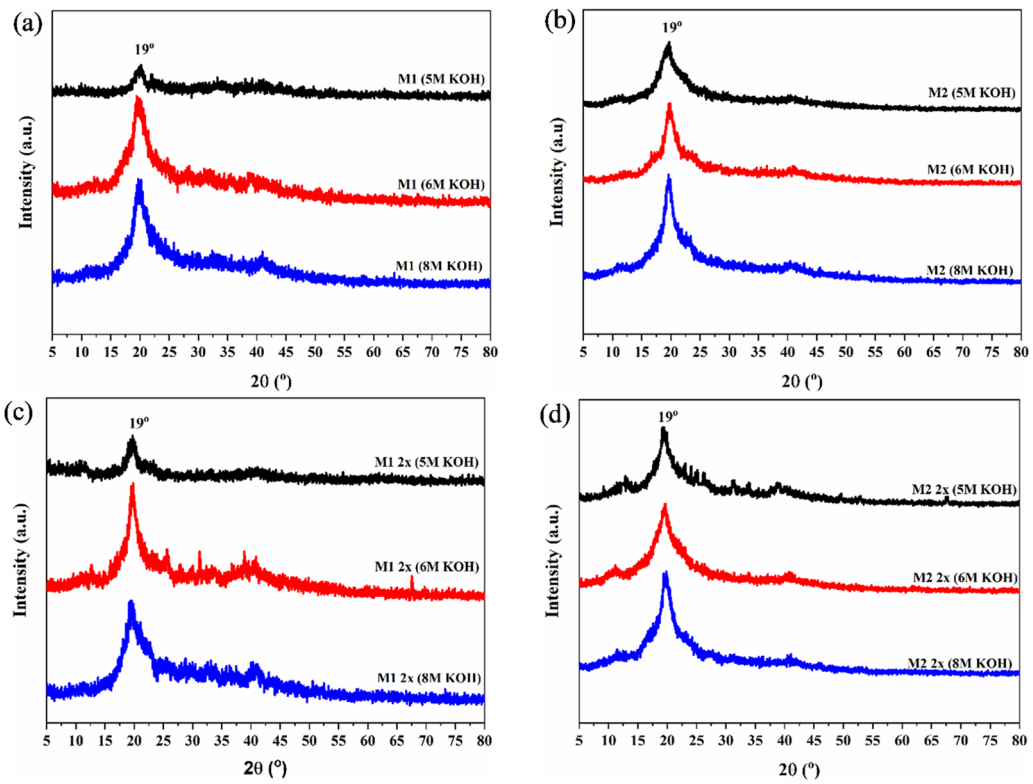

Fig. 3 XRD patterns of (a) M1, (b) M2, (c) M1 2x and (d) M2 2x samples under different KOH concentrations for activations.

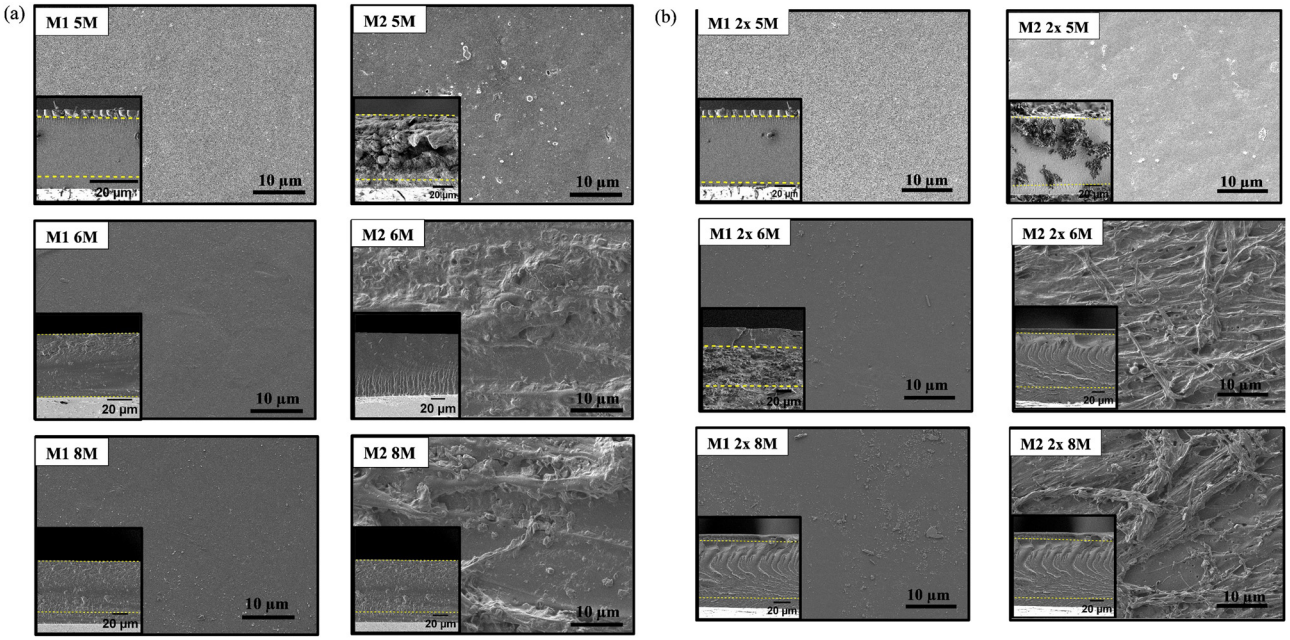

Fig. 4 (a) SEM surface images (10k× magnification) and the cross-sectional images (500× magnification) of QPVA membranes subjected to *in situ* crosslinking (M1) techniques and *in situ* crosslinking without heating (M2) with different KOH concentrations. (b) SEM surface images (10k× magnification) and the cross-sectional images (500× magnification) of QPVA membranes subjected to combined crosslinking techniques (M1 2x) and external–external crosslinking (M2 2x) with different KOH concentrations of activation.

higher temperature activation, room temperature activation still maintained a reasonable degree of structural integrity.[41] M1 2x samples showed a change in morphology. At 5 M KOH, the surface appeared relatively smooth, similar to M1 samples. However, increased roughness and fibrous structures were observed at 6 M and 8 M KOH concentrations. M2 2x samples (*in situ* and *ex situ* crosslinking, room temperature activation) exhibited more pronounced roughness compared to M1 2x samples, especially at higher KOH concentrations. The observed roughness and fibrous structures in M1 2x and M2 2x samples suggest increased crosslink density and potential improvements in mechanical properties.[42]

SEM observations confirmed the presence of KOH crystals as surface defects that can hinder efficient ion transport. While higher KOH concentrations and combined crosslinking methods enhance ion transport capabilities in QPVA membranes, optimizing KOH concentration to prevent excessive crystallization is crucial for overall membrane performance.

The thermal stability and decomposition behavior of QPVA membranes were assessed using thermogravimetric analysis (TGA). TGA curves (Fig. 5) revealed distinct weight loss stages depending on the crosslinking method and KOH concentration. The TGA results revealed only a 5–10 °C difference in onset temperatures between the crosslinked samples, indicating minimal variation in thermal stability. This can be attributed to the consistent crosslinking chemistry across all samples, as glutaraldehyde (GA) was used as the crosslinking agent in each case. The similar crosslinking mechanism and network structure limit the impact of crosslink density on the thermal decomposition behavior. Additionally, the KOH activation process may have introduced similar conditions for thermal degradation, further contributing to the small differences in onset temperature. As a result, while crosslinking improves stability, the overall thermal degradation mechanism remains largely uniform, leading to only slight variations in thermal stability between the samples.

Initial weight loss below 120 °C, attributed to unbound and bound water loss, is typical for hydrated membranes.[43] A significant weight loss occurs between 250 and 400 °C, corresponding to the thermal decomposition of the PVA backbone and the elimination of hydroxyl (OH) and amine (NH) groups of QPVA. This indicates the thermal stability of the crosslinked network. High-temperature decomposition between 450 and 550 °C is associated with the decomposition of residual carbonaceous materials. M1 samples exhibited higher thermal stability than unactivated samples, likely due to a more stable crosslinked structure. For M1 samples (5 M, 6 M, and 8 M KOH), the first onset temperature (T_{onset1}) was consistently 215 °C. The second major weight loss (T_{onset2}), corresponding to 60% weight loss, occurred at 405 °C. Char content at 600 °C increased from 5.87% (unactivated M1) to 13.28%, 10.94%, and 9.53% for 5 M, 6 M, and 8 M KOH, respectively. M2 samples showed lower thermal stability than M1 samples, suggesting less effective crosslinking. For M2 samples (5 M, 6 M, and 8 M KOH), T_{onset1} was 205 °C, while T_{onset2} (60% weight loss) occurred at 407 °C.

Combined crosslinking significantly enhanced thermal stability, particularly at higher activation temperatures. For M1 2x samples (5 M, 6 M, and 8 M KOH), T_{onset1} was 215 °C, with 60% weight loss occurring at 386 °C (T_{onset2}). Char content at 600 °C

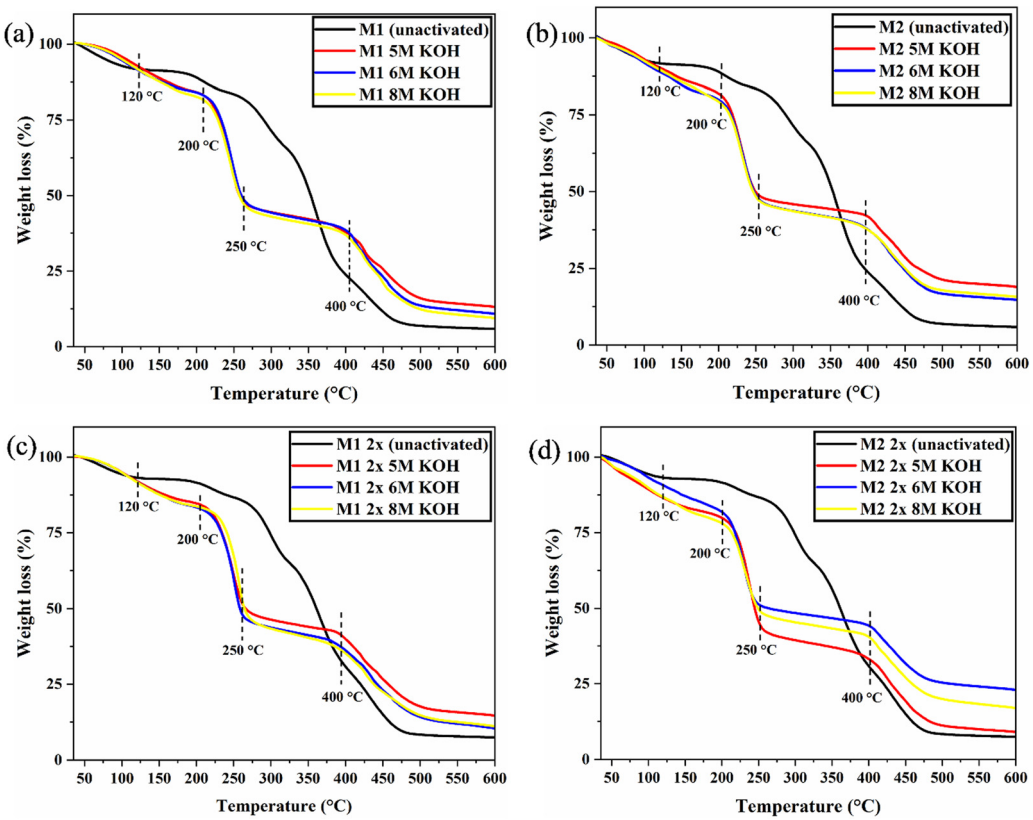

Fig. 5 TGA curves of (a) M1, (b) M2, (c) M1 2x and (d) M2 2x for comparison of unactivated and different KOH concentration of activation.

increased from 7.43% (unactivated M1 2x) to 14.70%, 11.14%, and 11.14% for 5 M, 6 M, and 8 M KOH, respectively. M2 2x samples showed improved stability over M2 but were less stable than M1 2x samples. For M2 2x samples (5 M, 6 M, and 8 M KOH), T_{onset1} was 205 °C, with T_{onset2} (56% weight loss) occurring at 405 °C.

Char content (remaining mass at 600 °C) provides insights into residual stability and carbon content. A higher char content generally indicates better thermal stability and higher crosslink density. Unactivated membranes showed low char content (5.87% for M1, 5.90% for M2). Activation significantly increased char content, peaking at 13.28% for 5 M KOH-activated M1 and 18.98% for 5 M KOH-activated M2. Combined crosslinking further improved the char content, with some variation depending on the KOH concentration and activation temperature. Higher activation temperatures (60 °C) promote more efficient crosslinking, leading to enhanced thermal stability. This condition is in agreement with the result reported by Zakaria and Kamarudin,[44] where the increase in thermal stability can be due to the strong interactions between the crosslinked polymer network and the QPVA matrix. This strong interaction expressed the enhancement in rigidity of macromolecular chains and resulted in more energy required for the movement of the polymeric chains, as reported by Liu *et al.*[45] Lower activation temperatures result in less effective crosslinking and lower stability.[46] A combined crosslinking approach, especially at higher activation temperatures, further enhances stability, highlighting the importance of optimizing crosslinking conditions.

The viscoelastic properties of QPVA membranes were evaluated using dynamic mechanical analysis (DMA). The storage modulus and tan delta of the unactivated and activated membranes are presented in Fig. 6. The storage modulus, E' of the M1/M2 QPVA membranes remains below 4.02×10^7 Pa, lower mechanical stability compared to the double crosslinked membrane. This is likely due to the less efficient crosslinking network formed and lower thermal stability, as observed in the TGA results. According to Lee *et al.*,[47] this lower mechanical stability can be linked to the less efficient crosslinking network formed. The double crosslinked QPVA membranes (M1 2x or M2 2x) show a significant improvement in storage modulus due to the two-step crosslinking approach. The storage modulus increases from approximately 4.02×10^7 Pa to 5.64×10^7 Pa, indicating enhanced rigidity of the QPVA polymer. This increase can be attributed to the additional crosslinking step, which provides a more robust and stable network structure.

The glass transition temperature (T_g) was determined from the tan δ peaks in the DMA curves. For the unactivated QPVA membranes (M1/M2), T_g is observed at 76 °C, while for the double crosslinked QPVA membranes (M1 2x/M2 2x), T_g decreases to 62 °C. This decrease in T_g for the double crosslinked membranes suggests increased segmental mobility due to the introduction of additional crosslinks, which may result in a more flexible polymer network. However, the overall

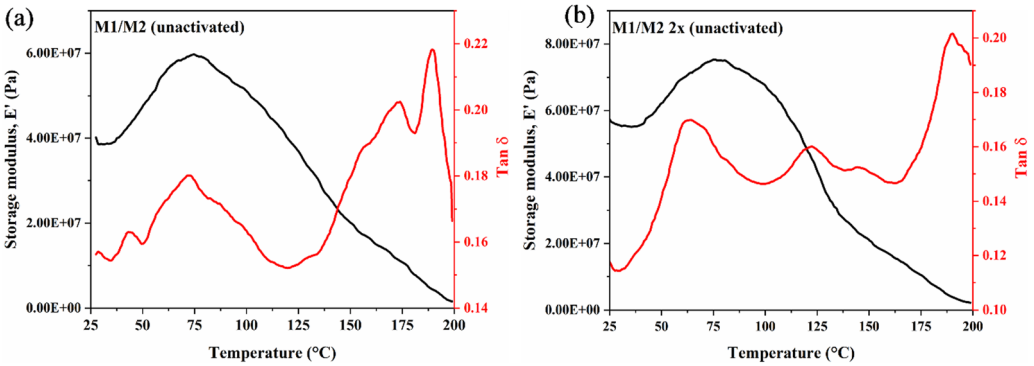

Fig. 6 DMA curve (a) M1/M2 (unactivated) and (b) M1 2x/M2 2x (unactivated) QPVA membranes.

rigidity and mechanical stability are enhanced due to the increased crosslink density, as reflected in the higher storage modulus.

Besides this, the strong drop in the storage modulus around 140 °C corresponds to the melting point of the QPVA membrane, indicating the transition from a solid to a viscous state. The tan δ curve for double crosslinked membranes shows a lower peak compared to unactivated membranes, reflecting a more stable crosslinked structure with lower damping characteristics. Furthermore, the tan delta curve for the double-crosslinked membranes exhibited a lower peak than the unactivated membranes, suggesting a more stable crosslinked structure with reduced damping characteristics. This is reflective of better mechanical stability and less energy dissipation during deformation. The humps after 100 °C indicate localized crystallization or phase separation between the amorphous and crystalline regions of the QPVA membrane. As the degree of crosslinking increases, these localized transitions become more pronounced, which is reflected in the multiple humps observed in the tan δ curve. Additional peaks or humps correspond to secondary relaxations or transitions related to different segments of the polymer network or interactions between the crosslinked regions and unreacted polymer chains. In the case of the double-crosslinked membranes (M1 2x or M2 2x), the higher crosslink density could lead to multiple relaxation processes as different segments of the polymer network exhibit varying degrees of mobility.

The DMA results correlate with the TGA findings, confirming that higher activation temperatures (60 °C) lead to enhanced crosslinking density and more thermally stable and mechanically robust membranes. This is evidenced from the higher decomposition temperatures and increased storage modulus for the activated membranes. Conversely, lower activation temperatures (room temperature) result in less efficient crosslinking, leading to membranes with lower decomposition temperatures, storage modulus, and mechanical stability.

3.2. Electrochemical properties of QPVA membranes

The electrochemical properties of QPVA membranes, including thickness, swelling degree, ionic conductivity, ion exchange capacity (IEC), and oxidative stability, were evaluated (Fig. 7). The following discussion correlates these properties with the thermal and mechanical analyses, providing a comprehensive understanding of QPVA membrane performance under different crosslinking and activation conditions. Swelling degree, indicating the membrane's water absorption ability, is inversely related to crosslinking density. According to Aladejana *et al.*,[48] the swelling of QPVA is reduced due to the formation of macromolecular crosslinking between PVA and glutaraldehyde. This crosslinking increases the density of the network, resulting in lower swelling degrees and higher mechanical stability. M1 samples generally exhibit lower swelling degrees than M2 samples (*e.g.*, M1 5 M KOH: 14.39%, M2 5 M KOH: 15.63%). Combined crosslinking (M1 2x and M2 2x) further reduces swelling, reflecting a denser network. This aligns with the increased storage modulus and reduced tan delta values observed in DMA, indicating enhanced stability.

Ionic conductivity is crucial for membrane performance. It varies significantly with the crosslinking method, KOH concentration, and equilibrium conditions in 1 M KOH, simulating AEMFC operation. M1 5 M KOH shows high ionic conductivity (40.93 mS cm^{-1} before equilibrium, 33.41 mS cm^{-1} after), indicating effective ion transport due to the stable crosslinked network. Other samples show varying ionic conductivity; M2 samples show lower ionic conductivity than M1 samples due to room temperature activation. Combined crosslinking shows mixed results, with some samples improving ionic conductivity after equilibrium. The variation before and after equilibrium highlights the importance of equilibrium conditions for evaluating their performance. High KOH concentration enhances ion transport properties due to strong chemical interactions (hydrogen bonding and induction forces) between KOH and QPVA.[27,30,49]

The water uptake (WU) reveals critical insights into the structural and functional characteristics of the QPVA membranes. A higher WU corresponds to greater water absorption, which directly correlates to ion conductivity.[50] For the M1 and M1 2x membranes, WU values of 48.8% and 29.4%, respectively, at 5 M KOH, demonstrate the impact of crosslinking density on water retention. The hydration number (λ), derived from WU and IEC, signifies the association of water molecules with ion exchange sites in the membrane.[51] For M1, the λ

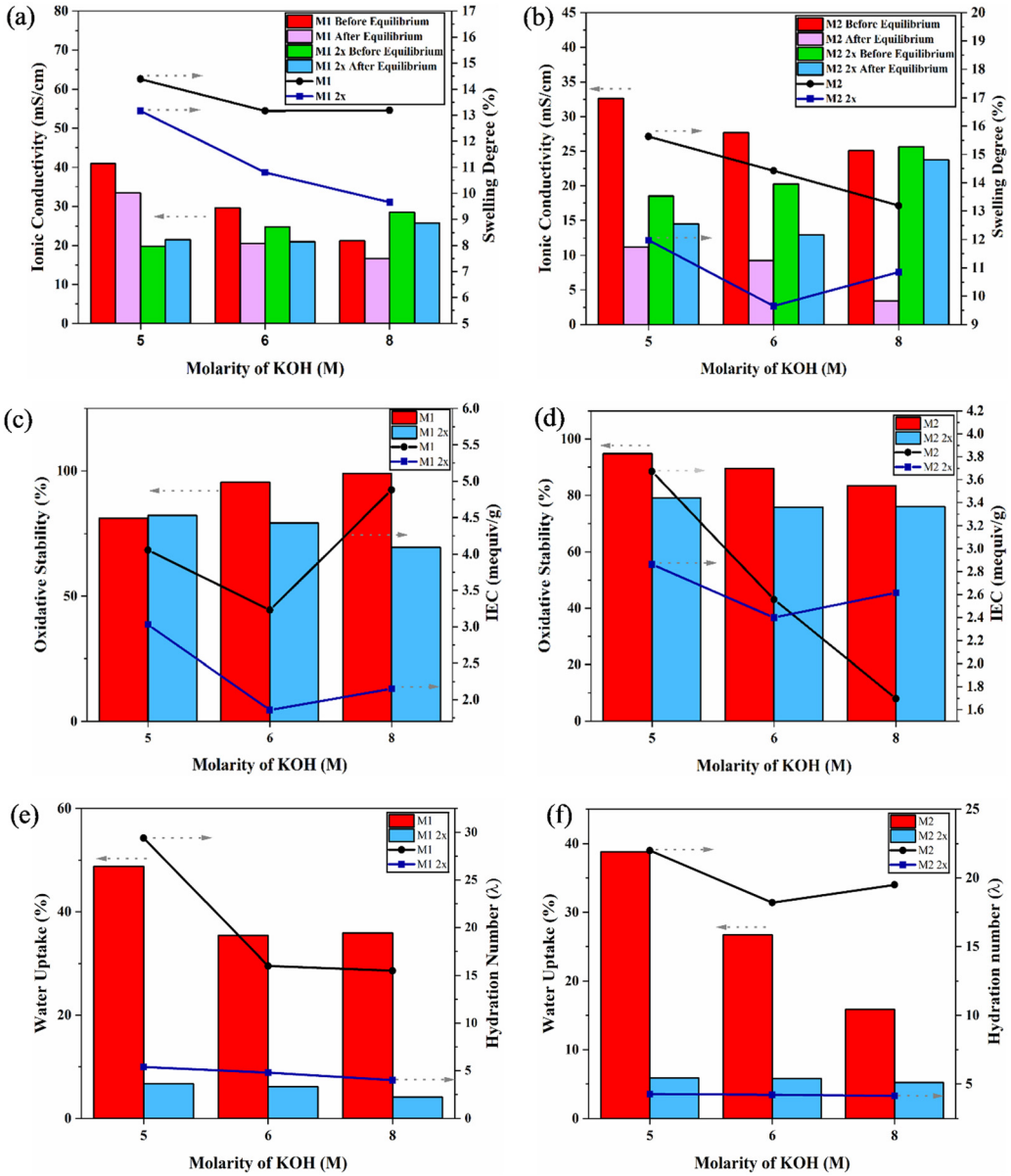

Fig. 7 (a) Ionic conductivity and swelling degree for M1 and M1 2x membranes at different KOH molarities. (b) Ionic conductivity and swelling degree for M2 and M2 2x membranes at different KOH molarities. (c) Oxidative stability and IEC values for M1 and M1 2x membranes at different KOH molarities. (d) Oxidative stability and IEC values for M2 and M2 2x membranes at different KOH molarities. (e) Water uptake and hydration number for M1 and M1 2x membranes at different KOH molarities. (f) Water uptake and hydration number for M2 and M2 2x membranes at different KOH molarities.

values at 5 M, 6 M, and 8 M KOH are 6.68, 6.09, and 4.08, respectively, reflecting the influence of crosslinking and activation on water retention. In contrast, M2 exhibits consistently lower λ values of 5.87, 5.79, and 5.21 under the same conditions, underscoring the less efficient crosslinking achieved at room temperature activation. Dual crosslinked membranes (M1 2x and M2 2x) show reduced WU and λ across all KOH concentrations due to the denser polymer network formed during the combined crosslinking process. The balance between WU and λ is critical for optimizing membrane performance. Although high hydration supports ionic transport, excessive water uptake can dilute charge carriers, reducing conductivity. In the dual crosslinked membranes, the reduced λ indicates tighter water binding, potentially stabilizing ionic transport while maintaining mechanical integrity. These findings suggest that the combined crosslinking process in M1 5 M KOH membranes effectively balances hydration and structural stability, leading to improved performance in anion exchange membrane applications.

While the quaternary ammonium groups formed in the membranes are generally stable under alkaline conditions, degradation can occur at high alkaline doping levels or elevated temperatures. This is primarily due to the susceptibility of certain bonds within the polymer network, such as C–O–C

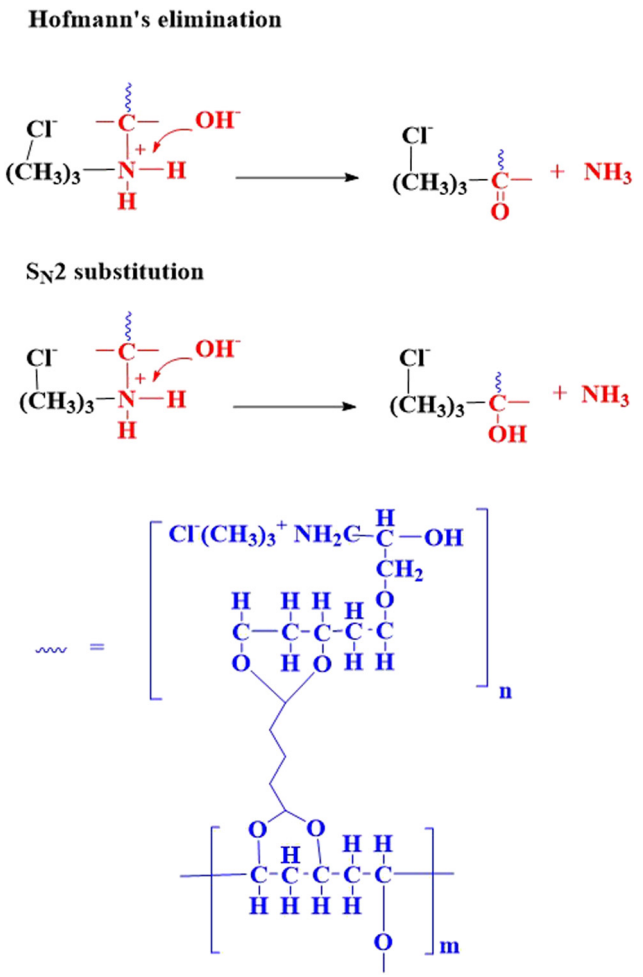

Fig. 8 Hofmann elimination and S_N2 substitution mechanism in QPVA membranes.

bonds, to nucleophilic attack. Under these extreme conditions, degradation mechanisms like Hofmann elimination and S_N2 substitution may take place, as illustrated in Fig. 8, leading to the breakdown of the polymer structure and a reduction in ionic conductivity and mechanical stability.[52] These mechanisms involve the breakdown of the polymer structure through various pathways, including the elimination of quaternary ammonium groups, formation of reactive intermediates, and nucleophilic substitution. This degradation results in reduced ionic conductivity and mechanical stability of the membranes. The presence of a hydroxyl group in the β-position of the quaternary ammonium salt side chain can further exacerbate the degradation of the polymer. This hydroxyl group, being an electron-withdrawing group, makes the β-carbon more susceptible to nucleophilic attack by hydroxide ions, thereby increasing the likelihood of degradation through pathways such as Hoffman Elimination and S_N2 substitution. These degradation mechanisms involve the breakdown of the polymer structure, particularly through the elimination of quaternary ammonium groups, the formation of reactive intermediates, and subsequent nucleophilic substitutions. However, it is important to note that this alkaline degradation is only one possible degradation pathway and does not necessarily occur under all operating conditions. The observed ionic conductivity and stability of M1 5 M KOH, even after equilibrium in 1 M KOH, suggest that the crosslinking strategy mitigates these degradation pathways under moderate conditions. Further optimization of the crosslinking density and membrane composition could enhance resistance to such degradation mechanisms, ensuring long-term performance in alkaline environments.

IEC reflects the membrane's ion exchange ability. M1 samples typically exhibit higher IEC values than M2 samples (*e.g.*, M1 5 M KOH: 4.055 mequiv g^{-1}, M2 5 M KOH: 3.672 mequiv g^{-1}), suggesting higher activation temperatures facilitate a more efficient ion-exchange network. Combined crosslinking shows mixed IEC trends, with excessive crosslinking potentially hindering ion exchange (M1 2x 6 M KOH: 1.857 mequiv g^{-1}).

Oxidative stability is the membrane's resistance to degradation under oxidative conditions. It is a critical parameter for AEMs because during operations like fuel cells and water electrolysis, reactive oxygen species (ROS), such as hydroxyl radicals ($^{\bullet}OH$) and hydrogen peroxide (H_2O_2), are formed as byproducts. These ROS can degrade the polymer backbone or functional groups within the membrane, compromising its ion transport properties, mechanical integrity, and overall durability. High oxidative stability ensures that the membrane maintains its performance and extends the operational lifespan of the fuel cell or electrolyzer system. M1 samples show higher oxidative stability than M2 samples, indicating higher activation temperatures enhance resilience. The oxidative stability of the QPVA membranes was investigated by measuring the residual weight percentage of each after treatment with Fenton's reagent. This assessment revealed distinct variations in oxidative stability across different crosslinking methods and KOH concentrations. M1 samples exhibited increased oxidative stability with higher KOH concentrations: 81.10% for M1 5 M KOH, 95.50% for M1 6 M KOH, and 99.00% for M1 8 M KOH. This suggests that higher KOH concentrations enhance crosslinking density, creating a stable polymer network that resists oxidative degradation. In contrast, M2 samples, which were *in situ* crosslinked without heating during activation, showed lower oxidative stability: 94.78% for M2 5 M KOH, 89.55% for M2 6 M KOH, and 83.48% for M2 8 M KOH. The absence of heat during activation led to less efficient crosslinking and a less robust polymer network. Double crosslinked samples showed varied oxidative stability. M1 2x 5 M KOH had an oxidative stability of 82.18%, decreasing to 79.28% for M1 2x 6 M KOH and further to 69.52% for M1 2x 8 M KOH. Similarly, M2 2x 5 M KOH had an oxidative stability of 79.05%, decreasing to 75.80% for M2 2x 6 M KOH and 76.06% for M2 2x 8 M KOH.

Combined crosslinking generally lowers oxidative stability, potentially attributed to two factors: (a) unreacted glutaraldehyde (GA) undergoing oxidation and forming carboxylic acids, leading to polymer degradation and reduced ionic conductivity,[53] (b) alkaline attack at the C–O–C bond causing bond scission. Oxidative stability was assessed using Fenton's reagent. M1 samples showed increased stability with higher

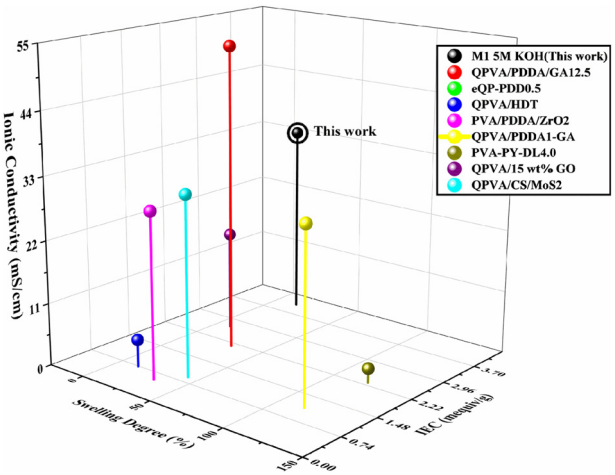

Fig. 9 Comparison of electrochemical properties of the AEM in this work and other PVA-based AEMs.[14,15,40–45] Note that: QPVA/PDDA/GA12.5: QPVA/poly(diallyldimethylammonium chloride)/12.5 wt% GA; eQP-PDDA0.5: electro-spun QPVA/0.5 wt% poly(diallyldimethylammonium chloride); QPVA/HDT: hexadecyltrimethylammonium bromide QPVA; PVA/PDDA/ZrO_2: PVA/poly(diallyldimethylammonium chloride)/ZrO_2; QPVA/PDDA1-GA: GA quaternized QPVA with 1 wt% poly(diallyldimethylammonium chloride); PVA-PY-DL4.0: pyridine functionalized-poly(vinyl alcohol)-1,4-dichlorobutane; QPVA/15 wt% GO: QPVA with 15 wt% of graphene oxide; QPVA/CS/MoS_2-0.2: QPVA/chitosan/0.2 wt% molybdenum disulfide nanosheets.

KOH concentrations, suggesting enhanced crosslinking density resists degradation. M2 samples showed lower stability due to less efficient crosslinking. Double crosslinked samples showed varied stability, with unreacted GA contributing to reduced stability. Carboxylate anions generated from carboxylic acids can compete with hydroxide ions for active sites on the anion exchange membrane (AEM), leading to reduced availability for hydroxide ions and thus lower ionic conductivity.

The performance of the synthesized M1 5 M KOH membrane was compared with those of other quaternized PVA-based AEMs to evaluate its suitability for AEM applications (as shown in Fig. 9). The key parameters considered were ionic conductivity, ion exchange capacity (IEC), and swelling degree. The M1 5 M KOH membrane exhibits an impressive ionic conductivity of 33.41 mS cm^{-1}, surpassing several other QPVA-based AEMs such as QPVA/HDT (4.8 mS cm^{-1})[54] and PVA-PY-DL4.0 (2.5 mS cm^{-1}),[55] demonstrating its effectiveness in ion transport. Although QPVA/PDDA/GA12.5 shows the highest ionic conductivity at 53.09 mS cm^{-1},[19] the M1 5 M KOH membrane's performance remains notable. The IEC of the M1 5 M KOH membrane is 4.05 mequiv g^{-1}, significantly higher than that of QPVA/PDDA/ZrO_2 (0.54 mequiv g^{-1})[56] and eQP-PDD0.5 (0.93 mequiv g^{-1}),[57] highlighting its enhanced ion exchange capabilities. The swelling degree of the M1 5 M KOH membrane is 14.39%, which is favorable compared to that of QPVA/PDDA1-GA (115%)[58] and eQP-PDD0.5 (9.4%).[57] This moderate swelling degree suggests balanced performance, ensuring mechanical stability without significantly compromising ionic conductivity. In summary, the M1 5 M KOH membrane demonstrates a high ionic conductivity, excellent IEC, and a moderate swelling degree, making it a well-balanced and effective material for AEM applications. These properties indicate that the M1 5 M KOH membrane is superior in many aspects to other QPVA-based AEMs, particularly in its ion exchange capacity and stability, which are critical for the efficient operation of anion exchange membrane fuel cells (AEMFCs).[59]

4. Conclusion

This study demonstrates that the choice of crosslinking techniques and activation conditions significantly impacts the structural and electrochemical properties of quaternized poly(vinyl alcohol) (QPVA) membranes. Utilizing glutaraldehyde as a crosslinking agent, both *in situ* and combined crosslinking approaches were systematically evaluated at varying KOH concentrations (5 M, 6 M, and 8 M). The combined crosslinking approach effectively suppressed membrane swelling and enhanced mechanical stability, while the *in situ* crosslinking at elevated temperature (60 °C) increased the crosslink density and ionic conductivity. Notably, the M1 membrane activated with 5 M KOH demonstrated the highest ionic conductivity (40.93 mS cm^{-1} before equilibrium and 33.41 mS cm^{-1} after equilibration in 1 M KOH), indicating its suitability for anion exchange membrane applications. However, reduced oxidative stability in the double-crosslinked membranes highlights the trade-off between the crosslinking density and oxidative stability. Future research should focus on the oxidative degradation caused by unreacted glutaraldehyde and further optimizing the crosslinking density to enhance both stability and conductivity. Investigating alternative crosslinking agents or additives that improve oxidative stability without compromising ionic transport could also provide valuable insights for next-generation anion exchange membranes.

Author contributions

Wei Keat Ng: data curation; investigation; writing – original draft; writing – review & editing. Chun Yik Wong: data curation; formal analysis; investigation; methodology. Nur Adiera Hanna Rosli: visualization; formal analysis; investigation; methodology. Kiranraj Vaiyanan Kannan: visualization; formal analysis; investigation. Kee Shyuan Loh: supervision; conceptualization. Bee Lin Chua: supervision; writing– review & editing; conceptualization. Wai Yin Wong: methodology; format analysis; supervision; writing – original draft; writing – review & editing.

Data availability

All data supporting the findings of this study, including synthesis methods, characterization results, and electrochemical data, are included and presented in this manuscript. No additional datasets were generated or analyzed.

Conflicts of interest

There are no conflicts of interest to declare.

Acknowledgements

This work is financially supported by Universiti Kebangsaan Malaysia through the project code DIP-2023-001.

References

1 W. Johnny, Everything you need to know about hydrogen in the clean energy transition, (accessed December 3, 2022).
2 H. A. Firouzjaie and W. E. Mustain, *ACS Catal.*, 2019, **10**, 225–234.
3 G.-M. Liao, C.-C. Yang, C.-C. Hu, Y.-L. Pai and S. J. Lue, *J. Membr. Sci.*, 2015, **485**, 17–29.
4 V. Vijayakumar, T. Y. Son, K. S. Im, J. E. Chae, H. J. Kim, T. H. Kim and S. Y. Nam, *ACS Omega*, 2021, **6**, 10168–10179.
5 T. Nemeth, T. Nauser and L. Gubler, *ChemSusChem*, 2022, **15**, e202201571.
6 M. Kumari, J. C. Douglin and D. R. Dekel, *J. Membr. Sci.*, 2021, **626**, 119167.
7 S. Gu, R. Cai and Y. Yan, *Chem. Commun.*, 2011, **47**, 2856–2858.
8 L. Yin, R. Ren, L. He, W. Zheng, Y. Guo, L. Wang, H. Lee, J. Du, Z. Li, T. Tang, G. Ding and L. Sun, *Angew. Chem., Int. Ed.*, 2024, **63**, e202400764.
9 S. S. Nagadarshan, H. Y. Harshitha, J. Pattar, M. H. Halashankar Swamy and H. N. Anil Rao, *Polymer*, 2024, **302**, 127025.
10 X. Li, Z. Wang, Y. Chen, Y. Li, J. Guo, J. Zheng, S. Li and S. Zhang, *J. Membr. Sci.*, 2023, **670**, 121352.
11 E. Abouzari-Lotf, M. V. Jacob, H. Ghassemi, M. Zakeri, M. M. Nasef, Y. Abdolahi, A. Abbasi and A. Ahmad, *Sci. Rep.*, 2021, **11**, 3764.
12 S. Ayaz, Z.-Y. Yao, Y. Yang and H.-Y. Yu, *J. Membr. Sci.*, 2023, **680**, 121736.
13 Y. Ji, H. Luo and G. M. Geise, *Phys. Chem. Chem. Phys.*, 2020, **22**, 7283–7293.
14 G. Merle, M. Wessling and K. Nijmeijer, *J. Membr. Sci.*, 2011, **377**, 1–35.
15 S. Gu, R. Cai, T. Luo, Z. Chen, M. Sun, Y. Liu, G. He and Y. Yan, *Angew. Chem., Int. Ed.*, 2009, **48**, 6499–6502.
16 G. Das, J. H. Choi, P. K. T. Nguyen, D. J. Kim and Y. S. Yoon, *Polymers*, 2022, **14**, 1197.
17 C. Wu, Y. Wu, J. Luo, T. Xu and Y. Fu, *J. Membr. Sci.*, 2010, **356**, 96–104.
18 A. Lewandowski, K. Skorupska and J. Malinska, *Solid State Ionics*, 2000, **133**, 265–271.
19 A. M. Samsudin and V. Hacker, *J. Electrochem. Soc.*, 2021, **168**, 044526.
20 Z. Zakaria, S. K. Kamarudin and S. N. Timmiati, *Nanoscale Res. Lett.*, 2019, **14**, 28.
21 C.-A. Tao, H. Zhang, J. Huang, X. Zou, H. Zhu and J. Wang, *Mater. Res. Express*, 2017, **4**, 085601.
22 D. Kuckling, A. Doering, F. Krahl and K. F. Arndt, in *Polymer Science: A Comprehensive Reference*, ed. K. Matyjaszewski and M. Moller, Elsevier, Amsterdam, 2012, ch. 8.15, vol. 8, pp. 377–413.
23 G. B. McKenna, in *Comprehensive Polymer Science and Supplements*, ed. G. Allen and J. C. Bevington, Elsevier, Amsterdam, 1989, ch. 10, vol. 2, pp. 311–362.
24 T. Mu, R. Liu, N. Shi, G. Wang and J. Yang, *ACS Appl. Polym. Mater.*, 2023, **5**, 7110–7119.
25 B. Zhao, Z. Zhang, J. Zhang, L. Wang, T. Wang, J. Dong, C. Xu and J. Yang, *Polymer*, 2023, **286**, 126404.
26 Z. Jiao, Y. Han, T. Wang, J. Dong, Y. Zhao and J. Yang, *J. Power Sources*, 2024, **623**, 235404.
27 N. Shaari, S. K. Kamarudin and Z. Zakaria, *Int. J. Energy Res.*, 2019, **43**, 5252–5265.
28 S. Farris, J. Song and Q. Huang, *J. Agric. Food Chem.*, 2010, **58**, 998–1003.
29 S. P. Ahirrao, P. S. Gide, B. Shrivastav and P. Sharma, *Res. Rev.: J. Pharm. Nanotechnol.*, 2014, **2**, 1–6.
30 D. L. Zugic, I. M. Perovic, V. M. Nikolic, S. L. Maslovara and M. P. Marceta Kaninski, *Int. J. Electrochem. Sci.*, 2013, **8**, 949–957.
31 J. Y. Chu, K. H. Lee, A. R. Kim and D. J. Yoo, *ACS Sustainable Chem. Eng.*, 2019, **7**, 20077–20087.
32 R. Gokulapriyan, I. Arunkumar, H.-K. Lee and D. J. Yoo, *ACS Appl. Energy Mater.*, 2023, **6**, 12549–12559.
33 R. Gokulapriyan, S. C. Karthikeyan and D. J. Yoo, *J. Mater. Chem. A*, 2024, **12**, 23880–23896.
34 R. Gokulapriyan, B. H. Kim, S. Vijayapradeep, S. Manigandan, I. Arunkumar and D. J. Yoo, *J. Membr. Sci.*, 2024, **700**, 122692.
35 H. Hendrawan, F. Khoerunnisa, Y. Sonjaya and A. D. Putri, *IOP Conf. Ser.: Mater. Sci. Eng.*, 2019, **509**, 012048.
36 S. K. Vineeth, R. V. Gadhave and P. T. Gadekar, *Open J. Polym. Chem.*, 2019, **9**, 86–99.
37 M. Pakizeh, M. Karami, S. Kooshki and R. Rahimnia, *J. Taiwan Inst. Chem. Eng.*, 2023, **150**, 105025.
38 J. Qian, C. Wang, X. Zhang, J. Hu, X. Zhao, J. Li and Q. Ren, *J. Membr. Sci.*, 2023, **685**, 121946.
39 Y. Gu, Y. Zhang, Z. Wang, D. Liu, Y. Wang, T. Dong, S. Wang, Z. Li, J. Wu and Y. Lei, *Ind. Chem. Mater.*, 2024, **2**, 141–153.
40 A. Thorat, R. Chauhan, R. Sartape, M. R. Singh and J. K. Shah, *J. Phys. Chem. B*, 2024, **128**, 3707–3719.
41 Z. Zakaria and S. K. Kamarudin, *Mater. Lett.*, 2021, **292**, 129651.
42 Z. Zakaria and S. K. Kamarudin, *J. Appl. Polym. Sci.*, 2019, **136**, 47526.
43 M. T. Musa, N. Shaari, S. K. Kamarudin and W. W. Yin, *J. Appl. Polym. Sci.*, 2023, **140**, e54560.
44 Z. Zakaria and S. K. Kamarudin, *Int. J. Energy Res.*, 2020, **44**, 8988–9000.
45 Y. Liu, Y. Shen, X. Li, Y. Liu, Y. Duan and K. Yang, *Chem. Eng. J.*, 2022, **446**, 136896.
46 J. Yang, X. Hu, X. Fang, L. Fan, G. Qin, Z. Zhang, J. Xu, Y. Liang and Q. Chen, *J. Membr. Sci.*, 2022, **650**, 120386.
47 D. Lee, J. Cho, J. G. Son and B. Yeom, *Composites, Part B*, 2022, **229**, 109467.
48 J. T. Aladejana, Z. Wu, D. Li, K. Guelifack, W. Wei, X. A. Wang and Y. Xie, *ACS Sustainable Chem. Eng.*, 2019, **7**, 18524–18533.

49 J.-S. Lin, W.-T. Ma, C.-M. Shih, B.-C. Yu, L.-W. Teng, Y.-C. Wang, K.-W. Cheng, F.-C. Chiu and S. J. Lue, *Energies*, 2016, **9**, 1003.
50 Y. C. Lei, J. Zhou, W. Zhou, Y. Wang, M. Zhang, A. Zhang and L. Wang, *Chem. Commun.*, 2024, **60**, 11000–11016.
51 T. Zelovich, D. R. Dekel and M. E. Tuckerman, *J. Membr. Sci.*, 2023, **678**, 121638.
52 D. Henkensmeier, W.-C. Cho, P. Jannasch, J. Stojadinovic, Q. Li, D. Aili and J. O. Jensen, *Chem. Rev.*, 2024, **124**, 6393–6443.
53 S. Hegde, B. Munavalli, D. Achari, R. Gowda and M. Kariduraganavar, *New J. Chem.*, 2024, **48**, 8799–8808.
54 K. Hari Gopi and S. D. Bhat, *Ionics*, 2018, **24**, 1097–1109.
55 X. Han, J. Wang and L. Wang, *J. Appl. Polym. Sci.*, 2019, **136**, 47395.
56 A. M. Samsudin and V. Hacker, *Polymers*, 2019, **11**, 1399.
57 A. M. Samsudin, M. Roschger, S. Wolf and V. Hacker, *Nanomaterials*, 2022, **12**, 3965.
58 X. Du, H. Zhang, Y. Yuan and Z. Wang, *Green Energy Environ.*, 2021, **6**, 743–750.
59 X. Jiang, Y. Sun, H. Zhang and L. Hou, *Carbohydr. Polym.*, 2018, **180**, 96–103.